Photodetachment of H⁻ from intense, short, high-frequency pulses

Hua-Chieh Shao and F. Robicheaux

Department of Physics and Astronomy, Purdue University, West Lafayette, Indiana 47907, USA
(Received 11 February 2016; published 17 May 2016)

We study the photodetachment of an electron from the hydrogen anion due to short, high-frequency laser pulses by numerically solving the time-dependent Schrödinger equation. Simulations are performed to investigate the dependence of the photoelectron spectra on the duration, chirp, and intensity of the pulses. Specifically, we concentrate on the low-energy distributions in the spectra that result from the Raman transitions of the broadband pulses. Contrary to one-photon ionization, the low-energy distribution maintains an almost constant width as the laser bandwidth is expanded by chirping the pulses. In addition, we study the transitions of the ionization dynamics from the perturbative to the strong-field regime. At high intensities, the positions of the net one- and two-photon absorption peaks in the spectrum shift and the peaks split to multiple subpeaks due to multiphoton effects. Moreover, although the one- and two-photon peaks and low-energy distribution exhibit saturation of the ionization yields, the low-energy distribution shows relatively mild saturation.

I. INTRODUCTION

The last decade has seen growing interest in exploring and characterizing the ionization mechanism from short, high-frequency laser pulses owing to advances of technology, like free-electron lasers [1] and high-harmonic generation [2], to provide coherent x-ray and extreme ultraviolet (XUV) pulses. With the intense light sources from the free-electron laser, exotic electronic states have been created and nonlinear x-ray absorption has been investigated. Highly charged xenon ions, Xe^{21+}, have been produced by absorbing more than 57 XUV photons in 10 fs [3]. In addition, fully stripped neon atoms from femtosecond x-ray pulses with intensities up to 10^{18} W/cm² have also been detected, and the ionization processes have been identified [4]. Double-core-hole states in atoms [4] and molecules [5] have been produced such that intensity-induced x-ray transparency has been observed. Furthermore, the target electronic states can transmute into different structures in intense high-frequency fields. Simulations show that the hydrogen anion acquires light-induced excited states and is stabilized such that the ionization rate decreases as the intensity increases [6,7].

Besides the ionization dynamics, ultrashort XUV pulses have been employed as pump-probe tools to study electronic motion in atoms and molecules [2,8]. The valence electronic motion in krypton ions initiated by a near-infrared laser has been recorded using the attosecond transient absorption technique [9]. The atomic coherence evolution has been traced in XUV-pump–XUV-probe schemes with the pulses on the order of 1-fs duration [10]. Recently, synchronized vacuum ultraviolet and XUV pulses from high-harmonic generation have been demonstrated, and attosecond pump-probe experiments with these pulses have been proposed [11].

Due to these diverse phenomena and applications, understanding the ionization dynamics for short, high-frequency pulses is necessary to better control the pump-probe processes and interpret the experimental results. In this paper, we study the ionization dynamics for the electron detachment from hydrogen anions by such pulses. We have performed simulations to examine the responses of photoelectron spectra with respect to the variations of laser parameters such as frequency, duration, chirp, and intensity. Here, high frequency means the energy of the photon is much larger than the binding energy of the target state, so one-photon absorption can ionize the target.

In particular, we focus on the low-energy distribution in the photoelectron spectra. One unique feature in the ionization by short, high-frequency laser pulses is the low-energy photoelectrons produced by Raman processes. Due to the large bandwidth of short pulses, a Raman transition is possible for a single pulse in which the target electrons are able to absorb and emit photons with different frequencies to populate states adjacent to the initial state. For Rydberg or weakly bound initial states, low-energy continuum states can be populated as well. This Raman process has been considered as a hole burning in the Rydberg state of barium [12] and in the 2s wave function of hydrogen [13]. The idea of hole burning is that photoabsorption occurs near the core, since the conservation of energy and momentum requires the absorption of the recoil momentum by the core. If a laser pulse is much shorter than the response time of the outer part of the electronic wave function, then the ionization process has been completed before an appreciable reaction of the outer part of the wave function. Hence, the electron density near the core can be depleted by a short, high-frequency pulse, and, accordingly, a hole is created in the wave function.

For a hydrogenic atom, the time scale for a (Rydberg) electron to respond to an external perturbation is set by its Kepler period of the orbit which relates to the energy difference from its neighboring states [12]. For a hydrogen anion, however, the interaction between the weakly bound electron and the core is a short-range potential. The ground-state wave function can extend beyond the range of the potential. Therefore, its response time can be different from that of hydrogenic atoms. Moreover, only one bound state is supported by the short-range potential, and the states populated through the Raman processes are the continuum states. Unlike the bound states, these free electrons escape from the hydrogen atom and may have their own time scale of motion. Hence, the reaction of the loosely bound electron of H⁻ to a short pulse may differ from that of a hydrogenic atom.

053414-1

In addition, we investigate the transition of ionization dynamics from the perturbative to the strong-field regimes. Demekhin and Cederbaum have studied the high-frequency ionization of hydrogen atoms with laser intensities above 10^{15} W/cm^2 [14]. They identified the importance of the dynamic Stark shift (or ac Stark shift) of the ground state in the ionization process. The spectrum is significantly modified because of the interference of ionized waves from the Stark-shifted state. Their simulations and analysis show that the Rydberg states participate in the ionization process and contribute to the Stark shift of the ground state, even though the energies of photons ($\approx$53.6 eV) are much larger than the binding energy of the hydrogen atom. In contrast, the hydrogen anion has only a single bound state, so H$^-$ provides a model to study the direct coupling of the ground and continuum states. We calculated the spectra from H$^-$ at different intensities. At high intensities the spectra are modified owing to the interference of ionized waves. However, the interference patterns cannot be fully accounted for by Demekhin and Cederbaum's [14] theory. Moreover, the low-energy distribution exhibits a different trend of ionization yields at high intensities.

This paper is organized as follows. In Sec. II, we discuss the numerical method and discuss the approximations used in the simulations. Then, in Sec. III A we present the spectra for photodetachment of H$^-$ with moderately strong vacuum ultraviolet (UV) pulses. The properties of the low-energy structure are discussed. Next, the transition of ionization dynamics as the laser intensity increases is presented in Sec. III B. Finally, we summarize the study in Sec. IV. Unless otherwise specified, we use atomic units throughout the paper.

II. SIMULATIONS

We numerically solved the time-dependent Schrödinger equation in the single active electron approximation to obtain photoelectron spectra from the detachment of hydrogen anions. The Schrödinger equation for the laser-anion system is

$$i \frac{\partial \psi(t)}{\partial t} = [H_0 + V(t)]\psi(t), \tag{1}$$

where H_0 is the Hamiltonian of the hydrogen anion and $V(t)$ describes the laser-anion interaction. For the hydrogen anion, we use a model potential [15] to describe the interaction between the loosely bound electron and the hydrogen atom. The model potential consists of three parts:

$$V_l(r) = -\left(1 + \frac{1}{r}\right)e^{-2r} + \frac{\alpha_d}{2r^4}\left(1 - e^{-(r/r_c)^6}\right) + v_l(r), \tag{2}$$

where $\alpha_d = 9/2$ a.u. is the static polarizability of the hydrogen atom, $r_c = 4.0$ a.u., and v_l is an angular momentum-dependent potential taking account of the low-energy scattering phase shifts for the partial waves with orbital angular momenta $l = 0$ and $l > 0$. See Ref. [15] for the functional form of $v_l(r)$. This potential has been used to study multiphoton detachment [15] and laser-induced rescattering [16] of H$^-$. The hydrogen atom is assumed to be infinitely heavy and centered at the origin. This model potential gives an H$^-$ binding energy of 2.773×10^{-2} a.u. (0.7546 eV), which agrees with the experimental value (0.754 20 eV) [17].

For the laser-anion interaction, we consider the dipole approximation in which the spatial dependence of the electric field and the magnetic field are neglected. Moreover, the length gauge is used, so

$$V(t) = -\boldsymbol{d} \cdot \boldsymbol{E}(t), \tag{3}$$

where $\boldsymbol{d}$ is the dipole operator and $\boldsymbol{E}(t)$ is the electric field of the laser pulse. We assume that the electric field is linearly polarized. Since few-cycle laser pulses are used in our simulations, in order to be consistent with the requirement of zero net force exerted on H$^-$ [18], the electric field in Eq. (3) is derived from a vector potential. We assume that the vector potential has a Gaussian envelope with a carrier frequency, ω:

$$\boldsymbol{A}(t) = -\frac{1}{\omega} \boldsymbol{E}_0 e^{-\frac{t^2}{2\sigma^2}} \sin\left(\omega t + \frac{\beta}{2\sigma^2}t^2\right), \tag{4}$$

where $\boldsymbol{E}_0$ is the peak amplitude of the electric field, σ is the Gaussian width, and β denotes the chirp. The energy of the photon ranges from 8 to 45 eV in our simulations.

The method of solving the time-dependent Schrödinger equation has been described elsewhere [19], so we only summarize it here. The wave function is expanded in spherical harmonics $Y_{lm}(\hat{\boldsymbol{x}})$:

$$\psi(\boldsymbol{x},t) = \sum_{lm} \frac{u_{lm}(r,t)}{r} Y_{lm}(\hat{\boldsymbol{x}}), \tag{5}$$

where $r = |\boldsymbol{x}|$. Then the reduced radial wave functions $u_{lm}(r,t)$ are propagated on a radial-angular momentum grid using the Crank-Nicolson and split-operator schemes. We used a square-root radial grid, whose mesh points are denser close to the origin, to take account of the rapid oscillation of the wave functions near the core. The kinetic energy operator in H_0 is approximated by a three-point finite difference. The initial condition for $u_{lm}(r,t)$ is the ground state of H$^-$ whose orbital angular momentum $l = 0$. For a linearly polarized pulse, the magnetic quantum number m is conserved and remains equal to its initial value, $m = 0$, in our simulations. All simulations have been tested for convergence. The observable is the photoelectron spectrum dP/dE, namely, the probability of observing an electron at energy E per unit energy interval. It is calculated by projecting the wave functions $\psi(\boldsymbol{x},t_f)$ at the end of propagation onto the continuum states of H_0 [20].

III. RESULTS AND DISCUSSION

A. Photodetachment of H$^-$ by short UV pulses

A typical photoelectron spectrum for detachment of H$^-$ by a short, high-frequency laser pulse with linear polarization is shown in Fig. 1. The Gaussian width of the pulse is $\sigma = 25$ a.u., corresponding to the full width at half maximum (FWHM) of 1.5 fs, and the frequency is $\omega = 0.29$ a.u. (8.0 eV). The strength of the electric field is $\boldsymbol{E}_0 = 0.05$ a.u. The spectra for s, p, and d partial waves are also shown in Fig. 1. The total spectrum shows a strong peak centered at energy 0.27 a.u., and two small peaks on either side. At the high-energy side a wider peak is located at 0.56 a.u., while an asymmetric peak resides just above the threshold. The inset of Fig. 1 depicts the details of this low-energy distribution. The partial-wave spectra show that the two side peaks have contributions from partial waves
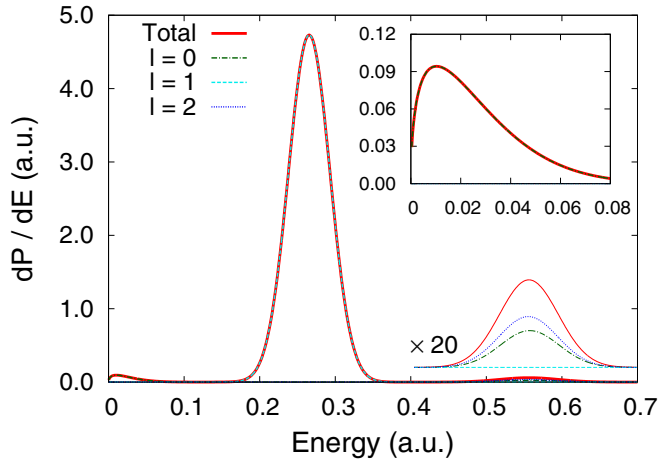
FIG. 1. The total and partial photoelectron spectra dP/dE resulting from detachment of H⁻ by a linearly polarized laser pulse with an 8-eV carrier frequency. The envelope of the vector potential is assumed to be a Gaussian distribution with a duration (FWHM) of 1.5 fs. The strength of the electric field is $E_0 = 0.05$ a.u., corresponding to the peak intensity 8.8×10^{13} W/cm². The red solid line is the total spectrum, and the partial spectra for the s, p, and d waves are represented by the green dash-dotted, cyan dashed, and blue dotted lines, respectively. The inset shows the low-energy distribution of the spectra due to the Raman process initiated by the short laser pulse. The spectra above 0.4 a.u. magnified by a factor of 20 are also shown. Note that the partial spectra for the s and p waves cannot be easily distinguished from the respective low-energy distribution and the main peak in the total spectrum.
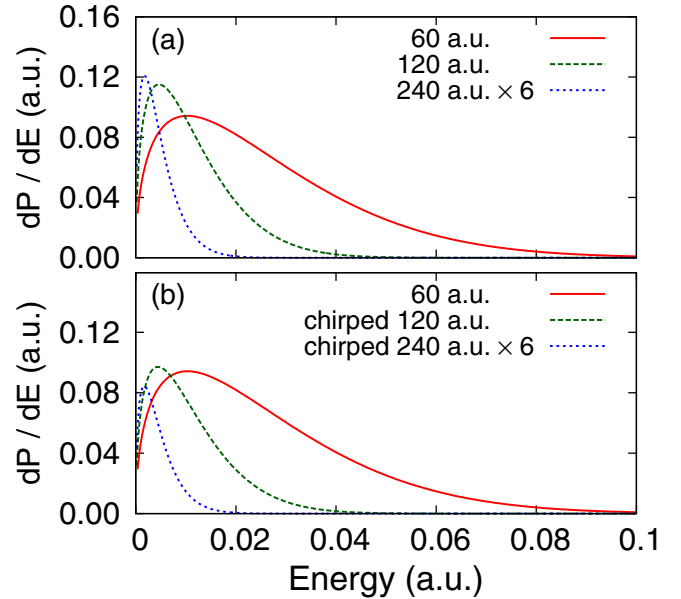

FIG. 2. Comparison of the low-energy distributions of (a) the spectra for the three transform-limited pulses with the following durations (FWHM), 60, 120, and 240 a.u., and (b) the spectra of unchirped 60-a.u., chirped 120-a.u., and chirped 240-a.u. pulses. The chirps of the 120-a.u. and 240-a.u. pulses are chosen such that all three pulses in panel (b) share the same bandwidth. The frequency of the laser pulse is 8 eV, and the peak amplitude is $E_0 = 0.05$ a.u. For purpose of comparison, the spectra of the 240-a.u. pulses in panels (a) and (b) have been multiplied by a factor of 6.

having parity opposite to that for the main peak. Specifically, whereas only p waves contribute to the main peak, mainly s waves contribute to the low-energy peak and both s and d waves contribute to the high-energy peak. Therefore, from the above energy and partial-wave analysis one can identify the numbers of net absorbed photons to be 0, 1, and 2 for the peaks from low to high energy.

1. The low-energy distributions and hole burning

As discussed in Sec. I, the Raman process initiated by a short laser pulse is the mechanism rendering the low-energy distribution. The s and d waves comparably contribute to the two-photon absorption peak, while the contribution from the d wave for the zero-photon peak is negligibly small. This is because the low-energy photoelectrons are more easily affected by the centrifugal potential which suppresses the transitions to states with high angular momenta. The sharp decrease of the transition probability for the zero-photon peak as the energy approaches zero is due to the Wigner threshold law [21] that the s-wave cross sections for short-range potentials are proportion to $\sqrt{E}$. Since the inset in Fig. 1 clearly shows that the low-energy distribution has predominately s-wave contributions, the low-energy distribution indeed obeys the threshold law.

In order to study the responses of the weakly bound electron to short pulses, photoelectron spectra as a function of pulse duration are simulated [13]. Note that the bandwidth is not a sufficient condition to set the pulse duration, because

the relative phases between the frequency components of the pulse also determine the length of the pulse. In order to distinguish the effects from the duration and from the bandwidth, simulations with transform-limited and chirped laser pulses are performed. The chirp is modeled by a quadratic term in t in the phase of the vector potential [cf. Eq. (4)]. By introducing chirp to a pulse, the pulse bandwidth is widened but the duration is maintained. We consider three pulse durations (FWHM) that are 60, 120, and 240 a.u., and the corresponding transform-limited bandwidths (FWHM) are 2.5, 1.26, and 0.629 eV, respectively. Note that the bandwidth of the 240-a.u. pulse is smaller than the energy spacing between the ground and continuum states. Figure 2 shows the effects of pulse duration on the low-energy distribution. In Fig. 2(a) all three pulses are transform limited, while in Fig. 2(b) the 120-a.u. and 240-a.u. pulses are chirped such that their bandwidths are the same as the unchirped 60-a.u. pulse. Here we chose $\beta = 1.73$ and 3.87 a.u. for the 120-a.u. and 240-a.u. pulses, respectively. In order to compare the shapes of the spectra with different pulse durations, the spectra for the duration of 240 a.u. have been multiplied by a factor of 6.

Comparison of Figs. 2(a) and 2(b) shows that the width of the low-energy distribution is insensitive to the increase of the bandwidth introduced by the chirp. For the transform-limited case in Fig. 2(a), the width of the zero-photon peak significantly decreases and the peak shifts toward threshold when the pulse duration lengthens. Since the accessible states through the Raman transition for a single pulse are directly confined by the laser bandwidth, the probabilities to

populate the continuum states are reduced considerably as the bandwidth narrows. On the other hand, for the chirped case in Fig. 2(b), although the bandwidths of the chirped pulses are large enough so that, in principle, the same continuum states can be populated as those populated by the unchirped 60-a.u. pulse (solid line), the widths of these zero-photon peaks (dashed and dotted lines) are still substantially similar to those of the transform-limited counterparts in Fig. 2(a). That is, despite the fact that all three pulses in Fig. 2(b) have the same bandwidth, the energy width of the zero-photon peak in the photoelectron spectrum deceases with increasing pulse duration.

The pulse-width dependence of the low-energy distribution can be understood from time-dependent perturbation theory, which is still applicable for ultraviolet radiation with intensities up to 10^{15} W/cm^2 [22]. Let the electric field of the laser pulse be

$$\boldsymbol{E}(t) = \boldsymbol{F}_0(t)e^{-i\omega t} + \overline{\boldsymbol{F}_0(t)}e^{i\omega t}. \qquad (6)$$

Then the Fourier transform of $\boldsymbol{E}(t)$ consists of two components:

$$\boldsymbol{E}(\nu) = \boldsymbol{E}^+(\nu) + \boldsymbol{E}^-(\nu), \qquad (7)$$

where

$$\boldsymbol{E}^+(\nu) = \frac{1}{\sqrt{2\pi}} \int dt\, e^{i(\nu-\omega)t}\, \boldsymbol{F}_0(t) \qquad (8)$$

and $\boldsymbol{E}^-(\nu) = \overline{\boldsymbol{E}^+(-\nu)}$. We assume that the bandwidth of the laser pulse is smaller than its carrier frequency ω, so $\boldsymbol{E}^+(\nu)$ is nonzero around ω. The lowest-order transition amplitude $T_{fi}^{(2)}$ for the Raman process from an initial state i to a final state f is

$$T_{fi}^{(2)} = i \sum_n P \int d\nu \frac{\boldsymbol{d}_{fn} \cdot \boldsymbol{E}^-(\varepsilon_{fi} - \nu)\boldsymbol{d}_{ni} \cdot \boldsymbol{E}^+(\nu)}{\varepsilon_{ni} - \nu}, \qquad (9)$$

where $\boldsymbol{d}_{ba}$ is the transition dipole moment from the state a to the state b, $\varepsilon_{ba} \equiv \varepsilon_b - \varepsilon_a$ is the transition energy, P denotes the Cauchy principal value, and the summation includes all intermediate states n. (For continuum intermediate states, the summation is interpreted as an integral.) If the chirp is modeled by a quadratic term in the phase of $\boldsymbol{E}(t)$, $\boldsymbol{E}^\pm(\nu)$ also carries a quadratic phase in ν. However, owing to the opposite sign of the phases in the absorption $(+)$ and emission $(-)$ processes, these quadratic phases cancel each other in the Raman transition. Therefore, the transition amplitude from the chirped pulse behaves like the one from the transform-limited pulse with the same duration. Thus, the width of the zero-photon peak directly reflects the pulse duration rather than the bandwidth.

2. The chirp dependence of the low-energy distribution

Although the width of the low-energy distribution is insensitive to the chirp of a pulse when the duration is fixed, we can see that in Fig. 2 the magnitude of the zero-photon peak is affected by the chirp. Here, we further study the chirp dependence of the Raman processes by comparing the photoelectron spectra from positively and negatively chirped pulses with fixed duration and intensity. Figure 3(a) presents the spectra of a transform-limited pulse and chirped pulses
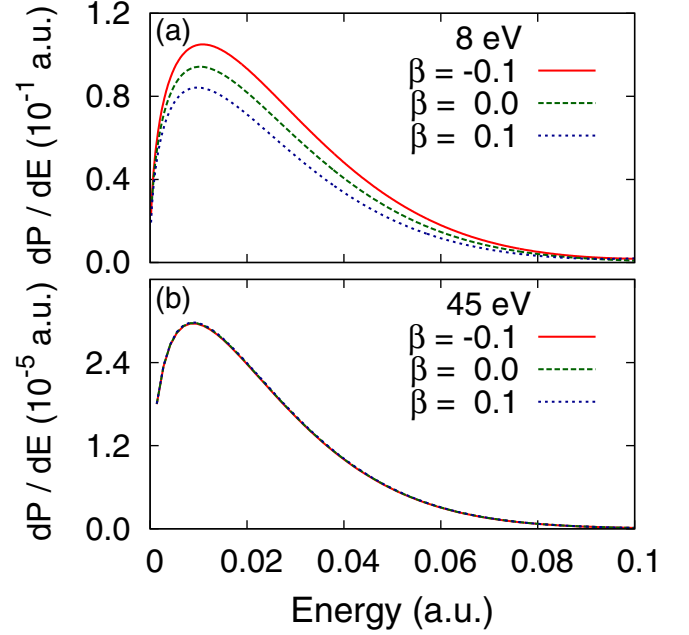

FIG. 3. Effects of the pulse chirps on the low-energy photo-electron spectra from the detachment of H$^-$ with (a) 8-eV and (b) 45-eV photon frequencies. The green dashed line represents the transform-limited pulse ($\beta = 0$ a.u.), while the red solid and blue dotted lines correspond to negative and positive chirps with a magnitude $|\beta| = 0.1$ a.u. See Eq. (4) for the definition of the chirp. Negative chirp means the instantaneous frequency decreases as a function of time. The strength of the electric field is $\boldsymbol{E}_0 = 0.05$ a.u., and the pulse duration (FWHM) is 60 a.u. in both panels.

whose magnitude of chirp is $|\beta| = 0.1$ a.u. Positive chirp means that the instantaneous frequency increases as a function of time. One can observe that the sign of chirp can enhance or suppress the zero-photon peak. The transition amplitude $T_{fi}^{(2)}$ suggests two possible sources causing the change of the magnitude of the zero-photon peak. The chirp of the pulse may be the dominant cause of this effect. Because of the nonzero detuning ε_{fi} of the emitted photon from the absorbed photon, the cancellation of the phases in the absorption and emission processes is incomplete. Therefore, the residual phases can interfere from the integration over the laser spectrum ν. On the other hand, since the continuum states participate in the Raman transition, the continuum structure of the H$^-$ can be another cause.

In order to determine the cause, we performed the same simulations except with a 45-eV photon, which is shown in Fig. 3(b). Both laser pulses have the same chirps and duration, so only the carrier frequency ω in Eq. (6) is changed. Therefore, $\boldsymbol{E}^+(\nu)$ is only displaced and centered at 45 eV due to the property of the Fourier transform. Since the displacement of $\boldsymbol{E}^\pm(\nu)$ preserves its phase from the chirp, the residual phases in the numerator of Eq. (9) for the 45-eV pulse are the same as those in the 8-eV case. However, the intermediate states in the 45-eV case are raised to higher energy because of the energy denominator. Hence, in the integrand of Eq. (9) only the dipole matrix elements are changed for the 45-eV simulation. For such high energy the continuum states are essentially like free particles, so the transition dipole moment
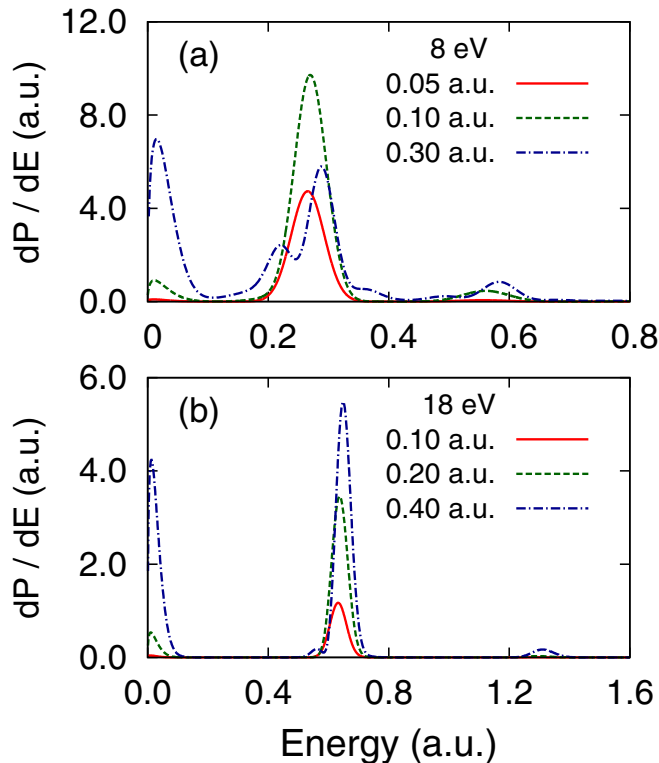
FIG. 4. Photoelectron spectra of the detachment of H⁻ by (a) 8-eV and (b) 18-eV photons as a function of peak electric amplitudes. Each curve represents a different electric field amplitude E_0 indicated by the legends. The pulse durations (FWHM) are 60 a.u. for both frequencies.

has weak dependence on the energy of the intermediate state. In Fig. 3(b) the curves with positive and negative chirps are almost identical, which implies the transition dipole moments are involved in the chirp dependence of the 8-eV case.

B. Multiphoton effects in the photodetachment of H⁻ by intense short pulses

When the laser intensity increases further, the photoelectron spectrum starts deviating from the perturbative behavior. The variations of the photoelectron spectra as the electric field strength increases are illustrated in Fig. 4 for 8- and 18-eV photons. For the 8-eV case in Fig. 4(a), the electric field increases from $E_0 = 0.05$ to 0.30 a.u., corresponding to the peak intensities 8.8×10^{13} and 3.2×10^{15} W/cm², respectively. One can observe that the peaks at each energy change significantly as the laser intensity increases. For the 18-eV case in Fig. 4(b), higher strengths of electric field ($E_0 = 0.10 \sim 0.40$ a.u.) are necessary to observe these nonlinear effects because of the higher frequency of the photon.

1. One-photon peak

We first discuss the response of the one-photon peak to the intense pulses. For the 8-eV pulse, the magnitude of the one-photon peak increases as the amplitude doubles from $E_0 = 0.05$ a.u., yet it then decreases as E_0 is further raised to 0.30 a.u. Meanwhile, multiple subpeaks can be observed. The subpeaks

emerge on both sides of the central peak, but the subpeak on the high-energy side ($E \approx 0.36$ a.u.) is much smaller than the one on the low-energy side ($E \approx 0.22$ a.u.) Moreover, the peak position is shifted upward as the intensity increases. The shift of the one-photon peak toward higher energy can also be observed for the 18-eV pulse. However, the subpeak appears at higher amplitude $E_0 = 0.40$ a.u. The relative magnitude between the subpeak and the central peak is smaller than the one in the 8-eV case, and the high-energy subpeak is hardly seen.

The splitting of the one-photon peak into multiple subpeaks at high intensity has been observed in simulations of multiphoton above-threshold ionization in a one-dimensional potential [23] and in ionization of hydrogen atoms by intense XUV laser pulses [14]. The shift of the peak position as a function of laser intensity is also seen in Ref. [14]. According to their analyses, the change of the peak position is due to the dynamic Stark shift. The initial state is dressed by the presence of the intense laser field, so its energy levels are shifted with respect to those of the continuum states. Then, the electron is ionized from this shifted initial state through a one-photon transition. The splitting of the one-photon peak is due to the dynamic interference of the ionized electron. The Stark shift follows the instantaneous intensity of the laser pulse. Therefore, given the energy of a final continuum state, the energy level of the one-photon dressed initial state crosses the energy twice at the leading and trailing edges of the pulse. Sharing the same energy, these ionized waves at two crossing times interfere with each other, which renders a modulation in the one-photon peak. If the Stark shift of the initial state is positive, then the interference occurs on the low-energy side of the main peak [14], and vice versa [23].

Since the Stark shift of the ground state for the model potential of H⁻ is positive at high frequency, the interference from ionized waves can explain the subpeak on the low-energy side for $E_0 = 0.30$ a.u. in Fig. 4(a). However, such a picture cannot simply explain the high-energy subpeak. Since the Stark shift depends on the laser intensity, the photoelectrons with higher energies are ionized around the peak of the laser pulse. Moreover, the ionization rate is larger around the peak of the pulse, so the number of ionized electrons should increase with energy, provided that the Stark shift and the decay rate of the initial state are smooth functions of the laser envelope. In contrast, the magnitude of the high-energy subpeak decreases rapidly.

Nevertheless, a simulation with longer pulse duration shows that the subpeaks are closer to each other. Since the modulation of the one-photon peak is due to the dynamic interference of emitted waves at different times of ionization with the same energy, the spacing between the subpeaks depends on the pulse duration. The accumulated phase difference between the two emitted waves is larger for a pulse with longer duration, so the modulation of the peak has a higher frequency of oscillation and, therefore, the subpeaks are more compact. Since the high-energy subpeak moves closer to the main subpeak for the pulse with longer duration, the high-energy subpeak indeed originates from the dynamic interference. However, a more complicated mechanism of interference may be involved in the strong-field detachment of H⁻ so that the magnitude of the high-energy subpeak is reduced.

One possible reason for a reduced high-energy subpeak is that the dynamic Stark shift may not simply follow the intensity profile of the laser pulse. Subcycle dynamic Stark shifts have been observed in the excited states of the helium atom [24]. The spectrogram from attosecond transient absorption shows that the absorption lines oscillate with a half-cycle period of the driving near-infrared pulse. Moreover, from the dynamic interference viewpoint, the multiphoton effect is only to dress the initial state such that its energy level is Stark shifted with some decay rate, followed by the ionization through a one-photon transition. However, for a strong field the initial state may be dressed by high-order Floquet-Fourier components.

In order to examine the dressing by high-order Floquet-Fourier components, we calculated the transition matrix elements [25]:

$$T_{fi} = -i \int dt (\phi_f(t), V(t)\psi_i^{(+)}(t)), \qquad (10)$$

where $\phi_f(t)$ is the final-state wave function and $\psi_i^{(+)}(t)$ is the solution of the time-dependent Schrödinger equation with the outgoing-wave boundary condition. Equation (10) can be interpreted as a transition amplitude from the dressed initial state i to the final state f through the one-photon transition indicated by $V(t)$. If the wave function $\psi_i^{(+)}(t)$ is approximated by a Stark-shifted initial state with a decay rate (that follows the intensity profile of laser), then Eq. (10) reduces to the same formulation in Ref. [14]. Here, however, we used the numerical wave functions for $\psi_i^{(+)}(t)$. Furthermore, $\psi_i^{(+)}(t)$ is decomposed into partial waves, so the dressing of each partial wave can be analyzed. Since the p wave dominates the one-photon peak, the final states $\phi_f(t)$ for the one-photon peak include solely the p-wave continuum states. Therefore, the transition matrix from the dressed partial waves to the p-wave continuum is written as

$$T_{fi}^p = T_{fi}^{p \leftarrow s} + T_{fi}^{p \leftarrow d}, \qquad (11)$$

where $T_{fi}^{p \leftarrow l}$ is the transition matrix element from the l partial wave of the dressed initial state i to the p-wave continuum of the final state f.

Figure 5 shows the total spectra $|T_{fi}^p|^2$ of the one-photon peak and the partial spectra $|T_{fi}^{p \leftarrow l}|^2$ from the dressed s and d waves as a function of the electric field amplitude $\boldsymbol{E}_0$ using Eq. (10) in the length gauge. One can observe that the relative contributions from the s and d wave switch as the intensity increases. For the lowest amplitude $\boldsymbol{E}_0 = 0.05$ a.u., the one-photon peak is predominately given by the transition from the dressed s wave. However, gradually contributing more as the amplitude increases, the transition from the dressed d wave outweighs that of the s wave at the highest amplitude [Fig. 5(c)]. Concurrently, both partial spectra show complicated multiple peaks, and the total spectrum of the one-photon peak splits to multiple subpeaks. The interference of the transition amplitudes from these Floquet-Fourier components of the dressed initial state may cause the involved modulation in the one-photon peak. Nevertheless, the analysis suggests that the dressing of the initial state involves more than a single angular momentum and possibly involves more than a single photon at $\boldsymbol{E}_0 = 0.30$ a.u.
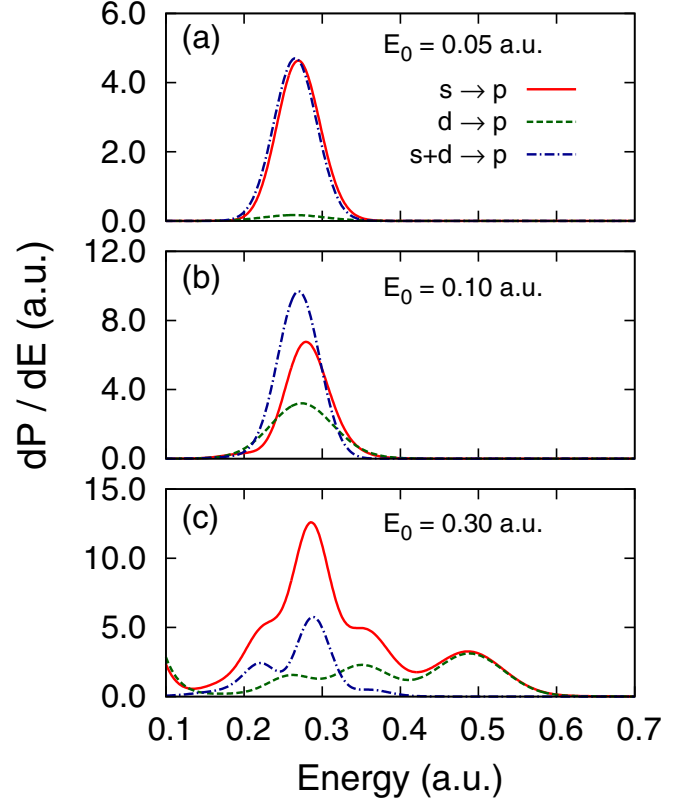

FIG. 5. Total and dressed partial-wave photoelectron spectra for the one-photon peak as a function of the electric field amplitude $\boldsymbol{E}_0$. The partial spectra $|T_{fi}^{p \leftarrow l}|^2$ from the dressed s and d waves are represented by the red solid and green dashed lines, respectively [cf. Eqs. (10) and (11)]. The total spectra $|T_{fi}^p|^2$ (blue dash-dotted lines), corresponding to the one-photon peaks in Fig. 4(a), are the absolute square of the amplitude that coherently sums the transition amplitudes $T_{fi}^{p \leftarrow l}$ from the dressed s and d waves. The pulse durations (FWHM) are 60 a.u., and the carrier frequencies are 0.29 a.u. (8.0 eV).

2. Zero- and two-photon peaks

Next, we compare the behaviors of the zero- and two-photon peaks in Fig. 4 as the amplitude of the electronic field increases. The magnitudes of both peaks show a stronger intensity dependence than that of the one-photon peak because of the higher-order processes involved. However, although both peaks are a second-order transition from the perturbative viewpoint, the zero-photon peak has a higher growth rate at $\boldsymbol{E}_0 = 0.30$ a.u. for the 8-eV pulse. One can observe that the magnitude of the zero-photon peak, barely being seen as $\boldsymbol{E}_0 = 0.05$ a.u., is comparable with the one-photon peak as $\boldsymbol{E}_0 = 0.30$ a.u. On the other hand, the two-photon peak exhibits only a moderate increment. This enhancement of the zero-photon peak can also be seen in the 18-eV case. In addition, for the 8-eV case the two-photon peak also shows multiple subpeaks at the highest electric amplitude, but no additional subpeaks appear in the zero-photon peak.

In order to quantitatively compare the relative yield of each peak as a function of intensity, we calculated the ionization probability for each peak by integrating the spectra over the energy range indicated in the legends of Figs. 6(a) and 6(b) for the 8- and 18-eV pulses, respectively. At low intensities, the
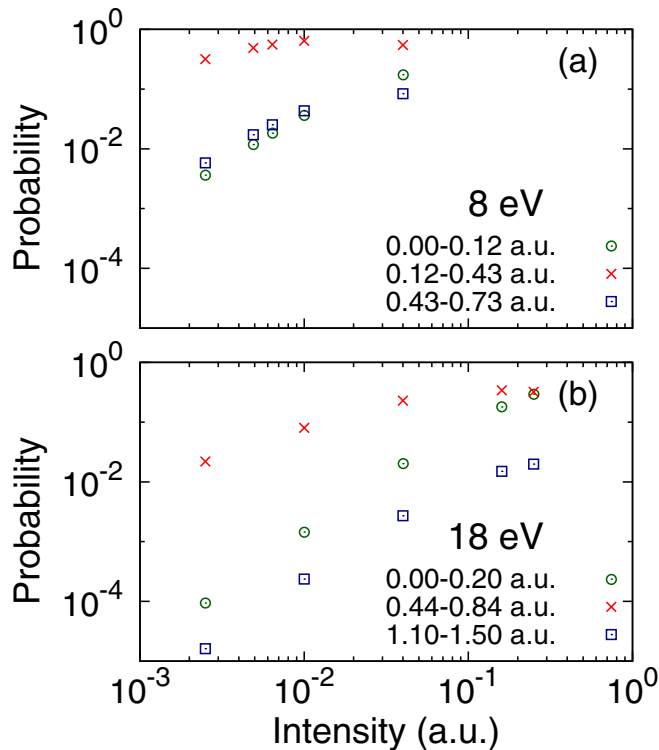
FIG. 6. The ionization yields for the zero-, one-, and two-photon peaks in the photoelectron spectra from the detachment of H⁻ as a function of peak intensity for (a) 8-eV and (b) 18-eV pulses. Green circle, red cross, and blue square symbols, respectively, represent the yields of the zero-, one-, and two-photon peaks. The energy intervals for integrating over the photoelectron spectra (cf. Fig. 4) are indicated by the legends in panels (a) and (b).

yields of all peaks show a relatively linear dependence on the intensity. The fitted slopes for the lowest three intensities of the zero-, one-, and two-photon peaks for the 8-eV (18-eV) pulse are 1.7 (1.9), 0.6 (0.8), and 1.6 (1.8), respectively. The slopes of the zero- and two-photon peaks are similar and close to 2, which is consistent with the perturbative description of second-order processes. At high intensities, however, the logarithms of the yields of all peaks show a nonlinear dependence on the logarithm of the intensity. The leveling off of the ionization probabilities indicates the saturation of the ionization yields. However, the zero-photon peak does not show the same level of saturation as that of the other two peaks. For the 8-eV case, the yields for the one- and two-photon peaks decrease at the highest intensity, but the slope for the zero-photon peak only decreases slightly. This is different from the multiphoton above-threshold ionization where the peak with the lowest energy in the spectrum is suppressed most at high intensities [26]. The reason for the mild saturation of the zero-photon peak may be that the

transitions of the zero-photon peak to the other states are bounded by the threshold, while the other multiphoton peaks can couple to other states by absorbing or emitting photons.

IV. SUMMARY AND CONCLUSIONS

In summary, we have performed simulations to study the photodetachment of H⁻ by short, high-frequency laser pulses. In addition to one- and two-photon ionization, a low-energy distribution can be seen in the photoelectron spectra that is caused by the Raman transition of the short pulses. The responses of the low-energy distribution differ from those of the one- and two-photon peaks as the laser parameters are varied. In the perturbative regime, the low-energy distribution maintains an almost constant width as the bandwidth of the laser is widened by chirping the pulse. Hence, the width of the low-energy distribution directly reflects the duration of the laser pulse. The same response of the low-energy distribution of H⁻ to a chirped pulse is also observed in the hydrogen atom [13]. Since this property can be understood by the cancellation of the phases in the absorption and emission processes of the Raman transition, such chirp dependence should apply for ionizations of other atoms by short, high-frequency pulses.

As the laser intensity increases to the nonperturbative regime, the yield of the zero-photon peak shows saturation milder than that of the yields of the one- and two-photon peaks. Moreover, the dynamic Stark shift of the ground state with respect to the continuum states can modify the spectrum. The position of the one-photon peak shifts as a function of laser intensity, and the peak splits to multiple subpeaks due to the dynamic interference of emitted waves at different ionization times. For the hydrogen anion, we found a modulation of the one-photon peak more involved than that of the hydrogen atom, which suggests more complicated multiphoton effects on a weakly bound system.

Finally, we note that autodetaching resonances have been observed near the H($n = 2$) threshold with the photon energy above 10.92 eV [27,28]. Since the single active electron approximation is employed, phenomena involving electron correlation cannot be described in our simulations. This is why the frequency of the laser pulse ($\omega = 8$ eV) is chosen away from these resonances. Moreover, although the effect of electron correlation on ionization dynamics is an interesting subject for future study, here we concentrate on the response of a weakly bound electron to the short, high-frequency pulses.

[1] B. W. J. McNeil and N. R. Thompson, Nat. Photonics **4**, 814 (2010).

[2] F. Krausz and M. Ivanov, Rev. Mod. Phys. **81**, 163 (2009).

[3] A. A. Sorokin, S. V. Bobashev, T. Feigl, K. Tiedtke, H. Wabnitz, and M. Richter, Phys. Rev. Lett. **99**, 213002 (2007).

[4] L. Young *et al.*, Nature (London) **466**, 56 (2010).

[5] J. P. Cryan *et al.*, Phys. Rev. Lett. **105**, 083004 (2010).

[6] H. G. Muller and M. Gavrila, Phys. Rev. Lett. **71**, 1693 (1993).

[7] M. Gavrila, J. Phys. B **35**, R147 (2002).

[8] R. Pazourek, S. Nagele, and J. Burgdörfer, Rev. Mod. Phys. **87**, 765 (2015).

[9] E. Goulielmakis *et al.*, Nature (London) **466**, 739 (2010).

[10] P. Tzallas, E. Skantzakis, L. A. A. Nikolopoulos, G. D. Tsakiris, and D. Charalambidis, Nat. Phys. **7**, 781 (2011).

[11] D. Fabris, T. Witting, W. A. Okell, D. J. Walke, P. Matia-Hernando, J. Henkel, T. R. Barillot, M. Lein, J. P. Marangos, and J. W. G. Tisch, Nat. Photonics **9**, 383 (2015).

[12] J. H. Hoogenraad, R. B. Vrijen, and L. D. Noordam, Phys. Rev. A **50**, 4133 (1994).

[13] P. L. Price, L. D. Noordam, H. B. van Linden van den Heuvell, and F. Robicheaux, Phys. Rev. A **89**, 033414 (2014).

[14] P. V. Demekhin and L. S. Cederbaum, Phys. Rev. A **88**, 043414 (2013).

[15] C. Laughlin and S.-I. Chu, Phys. Rev. A **48**, 4654 (1993).

[16] X. X. Zhou, Z. Chen, T. Morishita, A. T. Le, and C. D. Lin, Phys. Rev. A **77**, 053410 (2008).

[17] B. M. Smirnov, *Reference Data on Atomic Physics and Atomic Processes* (Springer-Verlag, Berlin, 2008).

[18] D. B. Milošević, G. G. Paulus, D. Bauer, and W. Becker, J. Phys. B **39**, R203 (2006).

[19] F. Robicheaux, J. Phys. B **45**, 135007 (2012).

[20] X. Chen, A. Sanpera, and K. Burnett, Phys. Rev. A **51**, 4824 (1995).

[21] E. P. Wigner, Phys. Rev. **73**, 1002 (1948).

[22] L. A. A. Nikolopoulos and P. Lambropoulos, Phys. Rev. A **74**, 063410 (2006).

[23] V. C. Reed and K. Burnett, Phys. Rev. A **43**, 6217 (1991).

[24] M. Chini, B. Zhao, H. Wang, Y. Cheng, S. X. Hu, and Z. Chang, Phys. Rev. Lett. **109**, 073601 (2012).

[25] V. P. Krainov, H. R. Reiss, and V. M. Smirnov, *Radiative Processes in Atomic Physics* (Wiley & Sons, New York, 1997), p. 215.

[26] G. Petite, P. Agostini, and H. G. Muller, J. Phys. B **21**, 4097 (1988).

[27] H. C. Bryant and M. Halka, in *Coulomb Interactions in Nuclear and Atomic Few-Body Collisions*, edited by F. S. Levin and D. A. Micha (Plenum, New York, 1996).

[28] H. H. Andersen, P. Balling, P. Kristensen, U. V. Pedersen, S. A. Aseyev, V. V. Petrunin, and T. Andersen, Phys. Rev. Lett. **79**, 4770 (1997).